

Article

Arsenic in a Karstic Paddy Soil with a High Geochemical Background in Guangxi, China: Its Bioavailability and Controlling Factors

Xuezhen Li¹, Xudong Ma¹, Qingye Hou¹, Xueqi Xia¹, Bo Li¹, Kun Lin¹, Xu Liu², Zhiliang Wu¹, Wenbing Ji³, Lei Wang⁴, Tao Yu^{5,6,*} and Zhongfang Yang^{1,6,*} 

¹ School of Earth Sciences and Resources, China University of Geosciences, Beijing 100083, China

² Ministry Environmental Protection Key Laboratory of Eco-Industry, Chinese Research Academy of Environmental Sciences, Beijing 100012, China

³ Nanjing Institute of Environmental Sciences, Ministry of Ecology and Environment, Nanjing 210042, China

⁴ Guangxi Bureau of Geology and Mineral Prospecting and Exploitation, Nanning 530023, China

⁵ School of Science, China University of Geosciences, Beijing 100083, China

⁶ Key Laboratory of Ecological Geochemistry, Ministry of Natural Resources, Beijing 100037, China

* Correspondence: yutao@cugb.edu.cn (T.Y.); yangzf@cugb.edu.cn (Z.Y.)

Abstract: Arsenic (As) is of widespread concern, as its elevated contents in soil and water have a serious impact on the ecological environment and human health. Soils in karst regions are characterized by a high geochemical background of As. However, the bioavailability of As in paddy soils and the potential risk of As transfer from the soil to rice remain unclear. In this study, 305 paired soil–rice samples were collected from karst regions in Guangxi, China, in order to examine the controlling variables and As bioavailability in the soil–rice system. According to this study, the karst region’s paddy soil had higher As concentrations than the non-karst region’s paddy soil. The As concentration in the rice grains was low, with only 0.62% of the rice samples exceeding the permissible value of inorganic As (0.2 mg/kg). Arsenic in the karstic paddy soils existed mainly in the residual fraction, while the water-soluble and exchangeable fractions, which are readily absorbed by rice, accounted for a relatively small proportion. The high content but low bioavailability of As in the karstic paddy soil was mostly attributed to the abundant Fe–Mn nodules, which contributed 64.45% of the As content in the soil. Within the Fe–Mn nodules, As was primarily bound to Fe-(oxyhydr)oxides, which could be released into the paddy soil under certain reduction conditions via the reductive dissolution of Fe-(oxyhydr)oxides. Under the natural pH conditions of the karstic paddy soil (pH 4.9–8.38), the leaching of As was almost negligible, and As could be steadily retained within the Fe–Mn nodules. However, extremely acidic or alkaline conditions promoted the release of As from the Fe–Mn nodules.

Keywords: arsenic; paddy soil; bioavailability; Fe–Mn nodules; karst regions



Citation: Li, X.; Ma, X.; Hou, Q.; Xia, X.; Li, B.; Lin, K.; Liu, X.; Wu, Z.; Ji, W.; Wang, L.; et al. Arsenic in a Karstic Paddy Soil with a High Geochemical Background in Guangxi, China: Its Bioavailability and Controlling Factors. *Appl. Sci.* **2024**, *14*, 1400. <https://doi.org/10.3390/app14041400>

Academic Editor: Mauro Marini

Received: 30 December 2023

Revised: 29 January 2024

Accepted: 5 February 2024

Published: 8 February 2024



Copyright: © 2024 by the authors. Licensee MDPI, Basel, Switzerland. This article is an open access article distributed under the terms and conditions of the Creative Commons Attribution (CC BY) license (<https://creativecommons.org/licenses/by/4.0/>).

1. Introduction

Arsenic (As), a potentially toxic element to humans, is bioaccumulative and non-biodegradable in the natural environment [1–3]. Karst terrains occupy about 7–10% of the planet [4]. China has approximately 2 million square kilometers of karst landforms, distributed in various provinces and regions, with the majority located in the southern part of the country, particularly widespread in Guangxi, Guizhou, Yunnan, and Chongqing. Because of the high average background values of karstic landscape-formed soils, they are frequently enriched in As [5,6]. Since As can enter the food chain and endanger human health [7–9], its excess in karst soils has drawn considerable attention from the public in an effort to protect the environment, the ecology, and public health in karst regions [10–12].

The natural presence of As in soils is primarily influenced by the composition of geological parent materials [13,14]. It has been shown that there is a strong correlation

between As in soils in northwest Greece and geological parent materials and anthropogenic sources of pollution [4]. In karst areas, the heredity of a parent rock with a high heavy metal content (e.g., black shale, sulfide deposits, and coal measure strata) and secondary enrichment caused by the leaching and weathering of a parent rock with a low heavy metal content (e.g., carbonate rocks) during soil development may lead to an As content that is higher than the normal background [15]. This natural process may result in wide areas of soil exceeding the environmental quality standards for As [16]. Consequently, a certain proportion of cultivated fields in karst regions may fall under strict supervision and be unsuitable for agricultural production, leading to significant public concern and constraining the local agricultural economy [5,17].

The physico-chemical characteristics and chemical forms of heavy metals largely determine the potential mobility and bioavailability of As [18,19]. In comparison with the total content of As, the bioavailability of As is more closely related to plant absorption [20,21]. The primary reasons for soil heavy metal elements in karst regions are pedogenic processes, which cause the high geological background values in the area [22,23]. In their natural state, the reactivity of most heavy metals is relatively low. Nonetheless, there have been notable alterations in the physico-chemical characteristics of soils as a result of frequent human production activities, for example, in northwestern Greece [4], southern China [22], and southwestern China [23]. As a result, the amount of certain heavy metals that are readily available has increased, which poses a major risk to the safety of agricultural products [24]. To date, the majority of relevant studies concerning As bioavailability and transfer in the soil–plant system have primarily focused on localized areas or limited regions with anthropogenic contamination [25,26]. However, the bioavailability of soil As and the potential high transfer risk of As from the soil to rice remain unclear, particularly in regions with a naturally high As background.

Guangxi, a region of China with one of the most extensive distributions of karst regions and with a significant carbonate rock development [27], faces significant environmental concerns related to the heavy metal contamination of soil. Recent studies have verified that the combination of secondary enrichment and parental rock inheritance is responsible for the high accumulation of As in Guangxi's karstic soil [6]. Fe–Mn nodules are present in many agricultural soils in the karst areas of Guangxi, China [28,29]. Fe–Mn nodules share a common origin with the surrounding soils and are formed in situ by the cementation of Fe-(oxyhydr)oxides to the soil matrix components. It has been proven that soil Fe–Mn nodules, which are mainly composed of Fe-(oxyhydr)oxides, also have a strong adsorption capacity for heavy metal elements and control the migration, adsorption, and precipitation of heavy metal pollutants in the soil, thus affecting the bioavailability of heavy metals [28–30].

In this study, a total of 305 paired soil–rice samples were gathered from Guangxi's karst regions, spanning a sizable geographic area, in order to obtain a thorough understanding of the environmental chemical behavior of As in rice–soil systems. Various extraction reagents and experimental conditions were employed to obtain more information about the bioavailability of soil As. Therefore, the objectives of this study were to (1) identify the As concentrations in the soil and rice in karst regions in Guangxi; (2) determine the bioavailability of As in the soils; and (3) investigate the controlling factors of As bioavailability and its potential environmental implications.

2. Materials and Methods

2.1. Study Area and Sample Collection

The Guangxi Zhuang Autonomous Region is located in the southern part of China (104°26'–112°04' E, 20°54'–26°24' N) (Figure 1). It has high temperatures and an abundance of rain due to its subtropical monsoon climate. Carbonate rocks make up the majority of the study area, that is, about 42% of the total land area, and they are mostly found in Guangxi's middle and western regions [31].

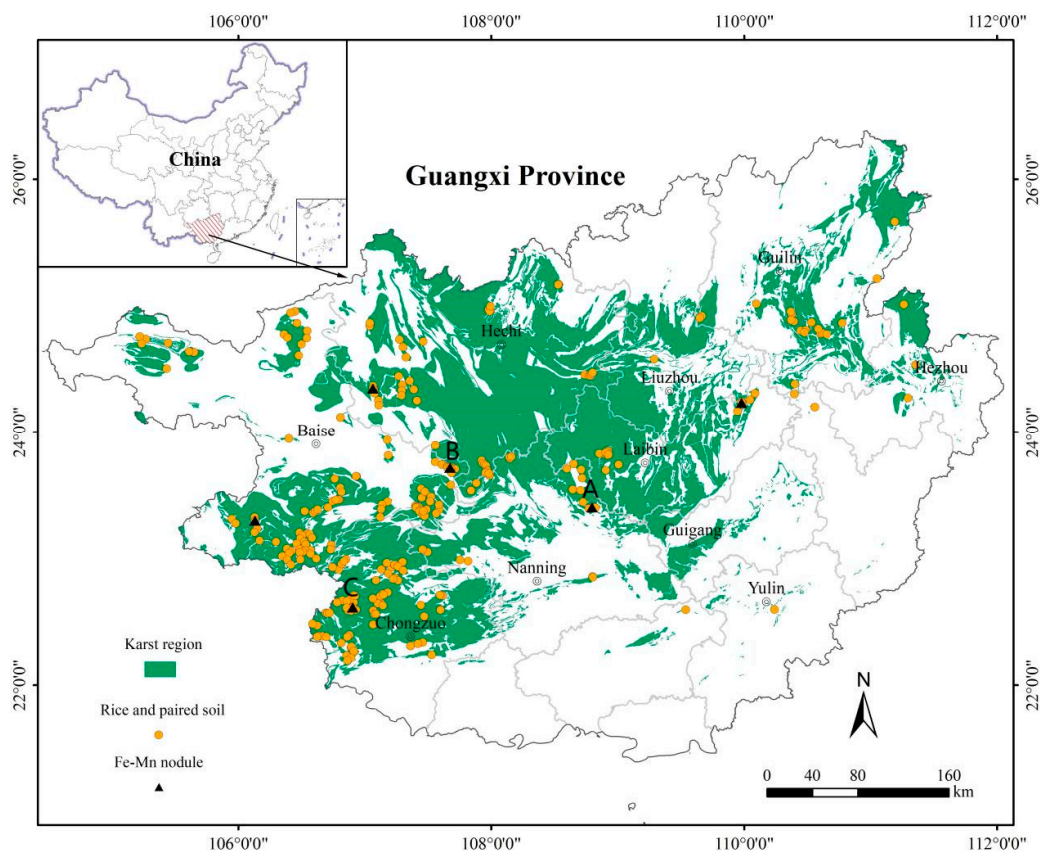


Figure 1. Sampling sites (yellow circles) from the karst region in Guangxi, China. (A, C): Mn nodules; (B): Fe nodules, the specific shapes of Fe-Mn nodules are shown in Figure 2.

In total, 305 paired soil–rice samples were obtained from the karst region in the study area in cooperation with the Guangxi Bureau of Geological and Mineral Exploration (Figure 1), and the samples were pre-processed in compliance with the Specification of Land Quality Geochemical Assessment [32]. Each rice sample consisted of an equal amount of rice grains from 3 sub-sampling points. The collected rice grains were placed in a mesh bag, hung in a cool place, air-dried, and then sent to the laboratory after threshing. Alongside the rice grain collection, the corresponding rhizosphere soil was also collected. After uprooting the rice roots, the soil adhering to the roots was shaken off. The depth of the rhizosphere soil collection depended on the depth of the rice roots. After uniformly mixing the soil shaken off from all sub-sampling points, the Four-Quarter Method was used to select a 1000 to 2000 g sample, which was then placed in a clean cloth bag and taken back to the base for air drying and processing. To minimize anthropogenic pollution inputs, the sampling locations were purposefully selected far from towns, highways, and mining regions.

Previous studies have shown that the enrichment of soil As in karst areas is closely related to the extensive development of Fe–Mn nodules in the soil [29,33]; therefore, six typical karst areas enriched with rooted soil As and where Fe–Mn nodules had extensively developed were selected in the study area (Figure 2), and the screening of the samples of Fe–Mn nodules with different diameters was carried out (Figure 1).

2.2. Sample Pretreatment and Chemical Analysis

Soil samples were first air-dried in a shady place and then passed through a 10-mesh (2 mm) nylon sieve to eliminate non-soil material (e.g., debris and plant residues). After being taken out of the husks, the rice grain samples were repeatedly rinsed in distilled water. After air drying at 25 °C, they were threshed, hulled, and crushed using a 60-mesh nylon sieve (0.25 mm).



Figure 2. The Fe–Mn nodules in the soil in the study area. (A,C): Mn nodules; (B): Fe nodules, the exact positional distribution of which is labelled in Figure 1.

For the soil samples passed through the 10-mesh nylon sieve, the Fe–Mn nodules with diameters > 2 mm were removed, and only those with diameters < 2 mm were retained as a soil component. Fe–Mn nodules with a diameter of more than 2 mm were eliminated from the samples that were sieved through a 10-mesh nylon sieve. Consequently, the Fe–Mn nodules with diameters lower than 2 mm were subjected to analysis. In consideration of previous studies and the presence of Fe–Mn nodules in the study area [34,35], we categorized the nodules into three groups based on the varying diameters: Group A (0.3–0.5 mm), Group B (0.5–1 mm), and Group C (1–2 mm). Each of the six samples underwent sieving through 10-mesh (2 mm), 18-mesh (1 mm), 35-mesh (0.5 mm), and 60-mesh (0.3 mm) nylon sieves to isolate the three groups of Fe–Mn nodules with different diameters. The quantity of each sample was documented for the three groups.

The concentrations of As in the soil samples were determined via atomic fluorescence spectrometry (AFS, AFS-9700, Kechuang Haiguang Instrument Co., Ltd., Beijing, China). TFe_2O_3 (total iron oxides), SiO_2 , Al_2O_3 , and K_2O were analyzed using X-ray fluorescence spectrometry (XRF, PW2440, Philips Co., Eindhoven, Netherlands). MgO, CaO, and Mn were analyzed via inductively coupled plasma–optical emission spectrometry (ICP-OES, iCAP 7400 Radial, Thermo Fisher Scientific Co., Cambridge, MA, USA). The sample was decomposed with HNO_3 , HClO_4 , and HF; dissolved with aqua regia (1 + 1); fixed in 25 mL polytetrafluoroethylene tubes and shaken well; and left to stand overnight. Soil organic carbon (SOC) was assessed using the potassium dichromate volumetric method [32,36]. The pH was assessed using ion-selective electrode methods [32,36]. The mineralogical compositions were determined using X-ray diffraction (XRD, BRUKER-D2 PHASER, Bruker Co., Karlsruhe, Germany) with the following parameters: target material: Cu; scanning speed: $2^\circ/\text{min}$; receiving gap: 0.03 mm; scanning surface range: $5\text{--}55^\circ$; step length: 0.02° ; accelerating voltage: 40 kV; and current: 200 mA. The chemical analysis method used for the Fe–Mn concretion samples, after grinding into powder, was the same as that used for the soil samples. The levels of As in the rice grains were measured using inductively coupled plasma–mass spectrometry (ICP-MS, iCAP Q, Thermo Fisher Scientific Co., Waltham, MA, USA): Weigh 0.2000 g of the dry specimen in a microwave digestion jar, add HNO_2 and MOS-grade H_2O_2 , tighten the lid, put the jar into a microwave digestion instrument for digestion, take out the digestion jar at the end of the reaction, put it on an acid catcher, evaporate it to a small volume, cool it and then transfer it to a 10 mL colorimetric tube, condense it with ultrapure water, and shake it well. As was measured using ICP-MS. Using reference standards, the analytical methods' accuracy was confirmed (GSS17, GSS19, GSS24, GSS28, GSB1, GSB4, GSB5, and GSB7) [32].

2.3. Sequential Extraction of As in the Soil

The seven-step sequential extraction procedures (SEP, amended Tessier Sequential Extraction) formulated by the China geological survey [37] were employed to investigate the fractions of As in the soil. This method divided As into seven fractions (F1–F7) [38]. The details of the fractionation and the SEP process are outlined in Table 1.

Table 1. Fractionation and seven-step sequential extraction procedures.

Fraction		Process
F1	water-soluble	2.5 g of sample and 25 mL of distilled water were mixed, shaken well, shaken for 30 min, centrifuged for 20 min, and filtered *
F2	exchangeable	25 mL MgCl ₂ was added to the residue, shaken well, shaken for 30 min, and centrifuged for 20 min
F3	bound to carbonates	25 mL NaOAc was added to the residue, shaken well, shaken for 1 h, and centrifuged for 20 min
F4	weakly bound to organic matter	50 mL Na ₄ PO ₇ was added to the residue, shaken well, shaken for 40 min, left for 2 h, and centrifuged for 20 min
F5	Fe/Mn oxide-bound	50 mL 0.25 M NH ₂ OH-HCl mixture was added to the residue, shaken well, shaken for 1 h, and centrifuged for 20 min
F6	strongly bound to organic matter	3 mL HNO ₃ and 5 mL H ₂ O ₂ were heated for 1.5 h at 85 °C + 3 mL of H ₂ O ₂ + 2.5 mL NH ₄ OAc-HNO ₃ , diluted to 25 mL, left for 10 h, and centrifuged for 20 min
F7	residual	the residues were dried, ground, and weighed; 2.0 g of the residue was digested with the 5 mL HCl-HNO ₃ -HClO ₄ mixture + 5 mL HF

* Centrifuge: Centrifugation for 20 min, 4000 rpm. Filter: The clear solution was filtered with a 0.45 µm filter membrane aperture, and the filtrate was used in a 25 mL colorimetric tube. Cleaning: Add about 100 mL of water to the residue, centrifuge for 10 min, discard the water phase, and retain the residue.

The recovery of SEP was based on a comparison of the sum of the seven fractions with the total content of As: Weigh 0.25 g of the sample accurate to 0.0001 g, place the sample in a 50 mL stoppered test tube, add a small amount of water to moisten it, add 10 mL (1 + 1) of aqua regia, cover with a stopper, and shake well. Add boiling water to the sample and leave it for 1 h, shake 2 times in the middle, take it out and cool it, fix the volume to 25 mL, shake well, and let it stand overnight. Dispense 5 mL of the clear solution in a small beaker, add 2.5 mL 1 g/L iron salt solution and 2.5 mL thiourea–ascorbic acid mixed solution, shake well, leave for 30 min, and use a KBH₄ solution as the reducing agent. As was determined using AFS, and it is expressed using the following equation (Equation (1)) [37,38]:

$$Recovery = \frac{F1 + F2 + F3 + F4 + F5 + F6 + F7}{Total} \times 100\% \quad (1)$$

The accuracy of the SEP analysis method was determined by conducting a full analysis of the elements in the soil as a standard and comparing the results with the sum of the fractions. The relative deviation (RE) was required to be ≤40% [37]. The pass rate for the single-element single-morphology analysis data was ≥85%.

$$RE\% = \frac{C_1 - C_0}{C_1} \times 100\% \quad (2)$$

where C₁ is the full amount of the element; and C₀ is the form of the element's total amount. The recovery ranged from 80.55% to 101.14%, and our study's RE values obtained following seven steps were lower than 10%; thus, these findings meet the requirements of standard DD2005-03 [37].

2.4. Selective Extractions and pH-Dependent Leaching Test

Selective extractions and pH-dependent leaching tests were conducted to identify whether these Fe–Mn nodules could be potential “Arsenic main sources” in soil [39,40]. Three extractants were utilized for the selective extractions of soil As, namely, acidified hydrogen peroxide (H₂O₂–HNO₃), hydroxylamine hydrochloride (NH₂OH–HCl), and citrate–bicarbonate–dithionite (CBD), aiming to elucidate the association of As with the Fe, Mn, and Al (oxyhydr) oxides in the Fe–Mn nodules [41,42]. Additionally, a control experiment was conducted using 0.5 mol/L HNO₃, which may dissolve some Al-containing minerals [35]. Hydroxylamine hydrochloride, known for its aggressive extraction properties,

targets As associated with easily reducible Fe and Mn oxides [43]. Acidified hydrogen peroxide extraction primarily involves dissolved Mn oxides [35]. CBD demonstrates a strong extraction capability for As bound to both amorphous and crystalline iron oxides [44].

The pH-dependent leaching test was adapted from the CEN/TS 14997 methodology [45]. A pH ranging from 2 to 11 was chosen for the experiment to analyze how As is released under different pH conditions. A total of 1 gram of the sample was placed in a 50 mL centrifuge PP tube, and 9.6 mL of deionized water was added to keep the ratio of liquid to solid (L/S) at 9.6, reaching a final value of roughly 10 when the acid and base were added. Ten pH values—2, 3, 4, 5, 6, 7, 8, 9, 10, and 11—were tested, including an extreme pH higher than that of typical soil. The pH levels were adjusted using HNO₃ (1 mol/L or 0.1 mol/L) and NaOH (2 mol/L or 1 mol/L). In every instance, a control experiment was carried out. For 48 h, the reactors were agitated. ICP-MS was then used to measure the leachate filtrate (Millipore® 0.45 µm) [28,35,39]. Table 2 describes the selective extraction procedure. Every extraction was carried out twice, using procedural blanks. The extracts underwent analysis for Fe, Al, Mn, and As using inductively coupled plasma–optical emission spectrometry (ICP-OES, iCAP 6500, Thermo Fisher Scientific Co., Taufkirchen, Germany), after being filtered through a 0.45 µm membrane filter.

Table 2. Detailed steps of the selective extraction procedure [35,41,42].

Extractant	Process
Control (HNO ₃)	The sample (100 mg) was placed in a container and mixed with 100 mL of 0.5 mol/L HNO ₃ . The container was placed at room temperature, stirring for 30 min.
Hydroxylamine hydrochloride (NH ₂ OH–HCl)	The soil (100 mg) was placed in a container and mixed with 200 mL of 0.1 mol/L NH ₂ OH–HCl (non-acidified, pH 3.6). The container was placed at room temperature, stirring for 2 h.
Acidified hydrogen peroxide (H ₂ O ₂ –HNO ₃)	The soil (100 mg) was placed in a container and mixed with 50 mL 30% of H ₂ O ₂ and 50 mL 1 mol/L HNO ₃ . The container was placed at room temperature, stirring for 30 min.
Citrate–bicarbonate–dithionite (CBD)	The soil (100 mg) was placed in a container and mixed with a solution containing 40 mL 0.3 mol/L sodium citrate (Na ₃ C ₆ H ₅ O ₇ ·2H ₂ O), 5 mL 1 mol/L sodium bicarbonate (Na ₂ CO ₃), and 1g sodium dithionite (Na ₂ S ₂ SO ₃). The container was placed in a 80 °C water bath and shaken for 1 h.

2.5. Data Analysis

Maps with geographic information were drawn using ArcGIS 10.8. Basic statistical analyses were carried out using SPSS 24.0 and Microsoft Excel 2021. The X-ray diffraction (XRD) pattern was analyzed with Jade 6.0. Other graphics were drawn using the OriginLab Origin v.2021.

The bioconcentration factor (BCF) is an important index to quantitatively calculate the accumulation of As in plant tissues from the environment [46,47]. The BCF is calculated as follows:

$$BCF = C_{\text{rice}} / C_{\text{soil}} \quad (3)$$

where C_{rice} is the As content in the rice (mg/kg); and C_{soil} is the whole As content in the soil (mg/kg).

The effect of nodules on soil heavy metal elements is manifested in two ways: the content of the element in the nodules of each grain size and the mass fraction of the element in the nodules of each grain size (i.e., the ratio of the mass of the element in the nodules of each grain size to the total mass of the element in the soil containing the nodules). To investigate the contribution of the nodules to the soil chemical composition and trace

element content, the parameter PQ (percentage of quality, %) was introduced and calculated as follows [48]:

$$PQ = \frac{\sum_{j=1}^j C_i \times M_j}{C_0 \times M_0 + \sum_{j=1}^j C_i \times M_j} \times 100 \quad (4)$$

where M is the mass of the nodule of particle size j, expressed in g; M_0 is the mass of the soil with the smallest particle size, expressed in g; C_i is the content of element i in the nodule of particle size j, expressed in mg/kg; and C_0 is the content of element i in the soil with the smallest particle size, expressed in mg/kg. The greater the value of PQ, the greater the proportion of the element present in the nodule and the greater the nodule's contribution of the element to the soil; the converse trend is observed with the smaller the value of PQ.

3. Results and Discussion

3.1. Soil Properties and As Concentrations

The average As concentration in the paddy soil (Table 3) was 23.49 mg/kg, higher than that in the non-karst area of Guangxi (12.01 mg/kg) [49]. The concentrations ranged from 2.36 to 162.92 mg/kg. Arsenic had a high degree of variability, as evidenced by its coefficient of variation (CV % = (standard deviation/mean) \times 100%) of 98.32% (>35%) [27]. The paddy soil's As content was greater than the background values of Guangxi (8.0 mg/kg) and the rest of the country (9.0 mg/kg) [50]. Moreover, compared with the published data on the As content in other regions and countries, the mean value of the paddy soil's As content in our study area was higher (Table 4). The median value of As in the study area was close to that in Hunan Province, China, and lower than that in French soils. However, the minimum values of As in Shanghai and Fujian, China, were greater than those in the study area (Table 4). Overall, the paddy soils formed by carbonate rocks had a high level of As enrichment, resulting in a higher geochemical background. Akun et al. [51] confirmed that Pleistocene carbonate-rich terrace deposits, pouri, are the cause of the elevated As concentrations.

Table 3. Descriptive statistic summary of the paddy soil properties (N = 305).

Statistics	Min	Max	Median	Mean	CV	Background Value of the Topsoil in Guangxi, China ^a	Background Value of the Topsoil in China ^a
As (mg/kg)	2.36	162.92	15.60	23.49	98.32	8.0	9.1
TFe ₂ O ₃ (%)	1.16	25.18	5.59	6.26	50.50	3.63	4.35
Mn (mg/kg)	29.9	2804.0	353.0	523.3	92.46	159	552
Al ₂ O ₃ (%)	5.04	28.27	14.01	14.57	28.69	13.07	12.96
CaO (%)	0.16	31.50	0.81	4.45	151.36	0.17	2.79
pH	4.97	8.38	7.18	7.04	13.83	5.15	7.15
SiO ₂ (%)	17.07	85.57	62.00	57.82	27.56	73.67	64.96
SOC (%)	1.16	6.30	2.60	2.80	35.69	1.29	1.15

^a The background value of the topsoil was obtained from Hou et al. [50].

Table 4. Arsenic concentration in the topsoil and rice from other regions/countries.

	Region/Country	N	Min	Max	Mean	Median	References
Topsoil (mg/kg)	Hunan, China	18,773	0.1	2670.1	19.5	13.0	[50]
	Jiangxi, China	15,547	0.4	19.2	8.4	8.0	
	Jilin, China	23,465	0.4	15.9	8.0	7.9	
	Shanghai, China	1744	4.6	11.4	7.9	7.9	[52,53]
	Fujian, China	14,682	4.7	3.9	0.1	13.5	
	France	2017	0.39	412.00	12.20	17.93	
	Italy	201	1.8	60	20	\	
	Cyprus	260	0.2	22.5	11.0	10.87	[51,54]

Table 4. Cont.

	Region/Country	N	Min	Max	Mean	Median	References
Rice (mg/kg)	Hunan, China	43	0.05	0.25	0.13	\	[55]
	Jiangxi, China	30	0.07	0.25	0.15	0.15	
	Guangxi, China	45	0.11	0.37	0.23	\	
	Jilin, China	4	0.09	0.16	0.13	0.13	
	Shanghai, China	34	0.01	0.16	0.11	0.11	
	Fujian, China	36	0.04	0.20	0.12	\	
	U.S.	163	0.03	0.66	0.25	0.25	[56–58]
	France	33	0.09	0.56	0.28	0.23	
	Bangladesh	144	0.02	0.33	0.13	0.13	
	Italy	38	0.07	0.33	0.15	0.13	
	Japan	26	0.07	0.42	0.19	0.18	
Egypt	110	0.01	0.58	0.05	0.04		

The paddy soil was primarily neutral with a median pH of 7.04, varying from 4.97 to 8.38. Notably, the median CaO content in the paddy soil was 0.81%, which was significantly higher than that in clastic and quaternary regions [38]. Research has revealed that elevated levels of Ca^{2+} ions in the soil are a principal cause of an increased soil pH [59]. An acidic environment could increase the soluble As content in the soil; however, the desorption of As from Fe (oxyhydr)oxides in alkaline environments might result in As(III) and As(V) mobility in the soil solution, which, in turn, increases As accumulation in rice [60]. Additionally, the TFe_2O_3 , Mn, and Al_2O_3 contents in the paddy soil were 6.62%, 523.30 mg/kg, and 14.57%, respectively, which were higher than the background values of Guangxi and the rest of the country; however, the SiO_2 content (57.82%) exhibited the opposite trend. This indicates the desilicification–allitization of paddy soils in karst areas. The soil organic carbon content ranged from 1.16% to 6.30%, with a mean value of 2.80%, regulating the solubility of As in the soil and thus affecting the bioavailability of As in rice [61,62].

3.2. Accumulation of As in Rice Grains

The land quality directly affects the quality and safety of crops, which, in turn, affect the health of those who rely on them. The As concentration in the rice grains ranged from 0.03 to 0.25 mg/kg, with a mean value of 0.11 mg/kg (Table 5), which was lower than that reported in many regions/countries (Table 4). Meharg et al. [58,63] reported that the average As content in rice was 0.14 mg/kg in China, and 81.64% of the rice samples containing As in our study area had As contents lower than this value. The BCF_{As} of the rice was 0.0084, which was considerably below that of other heavy metals, such as Cd, Zn, and Cu [11]. In summary, the As content in the rice grains remained low in the karst area.

Table 5. Arsenic concentration and BCF_{As} in rice grains ($N = 305$).

Statistics	Total As (mg/kg)	BCF_{As}	Inorganic As (mg/kg)
Min	0.03	0.0004	0.08
Max	0.25	0.0530	0.20
Median	0.10	0.0058	\
Mean	0.11	0.0084	\
REF ^a	\	\	0.62 ^b

^a REF (%) means the rate of exceeding the national food safety standard (GB2762-2017) [64]. ^b Seven rice grain samples with a total As concentration greater than 0.2 mg/kg were selected for the determination of inorganic As concentration, and the results show that the samples of inorganic As concentrations exceeded the standard.

Extensive studies on As speciation have demonstrated the coexistence of inorganic and organic As in rice [65,66]. Considering the greater levels of toxicity and carcinogenicity of inorganic As [67–69], the Ministry of Health of China states that the maximum permissible content of inorganic As is 0.2 mg/kg (GB2762-2017) [64]. Remarkably, just 0.62% of the rice

samples had inorganic As contents above the recommended level, a far lower percentage than the 4.0% in Guangxi's non-karst region [49]; however, the proportions of soil samples that exceeded the As risk screening values and risk intervention values were 31.46% and 1.31%, respectively (GB 15618-2018) (Figure 3) [16]. The As concentrations of most of the rice grains in the paddy soil with an above-standard As content were within the safety range. A high As content but low bioavailability in rice soils in the Guangxi karst region resulted in a low As accumulation in rice. If the existing standards are strictly enforced, the use of paddy soils with an As content exceeding the standards will be restricted in agricultural production, and this is wrong and unscientific. Therefore, it is imperative to explore the causes of the low bioavailability of soil As and provide scientific support for the management of agricultural soil quality.

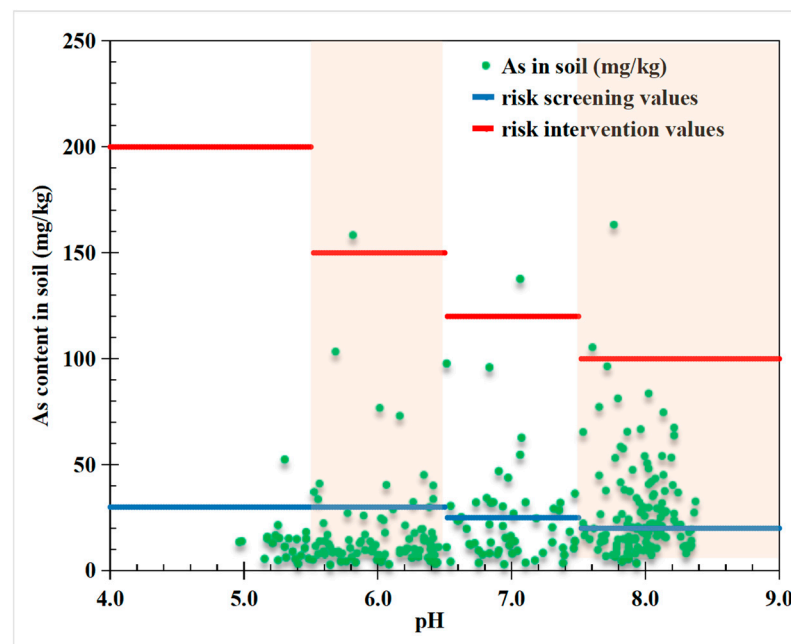


Figure 3. Arsenic content in the root soil under different pH values [16].

3.3. Arsenic Bioavailability in Paddy Soils Determined Using the Sequential Extraction Procedure

The bioavailability and mobility of As are closely related to its geochemical speciation, which is indicated by the extractable fraction [70,71]. Each As fraction is diverse in mobility and bioavailability [72]. In this study, the first two fractions (F1 and F2) were mobile and unstable and thus considered the bioavailable fractions for rice [70,73].

As shown in Table 6, As in the paddy soil existed mostly as the residual fraction (F7) in the karst area, accounting for 76.96%. F7 is considered stable in mineral crystal lattices and is unavailable for plants [73]. The proportions of other fractions (F3, F4, F5, and F6) were F4 (11.73%) > F5 (8.07%) > F6 (1.19%) > F3 (0.97%) > F1 (0.56%) > F2 (0.51%). The water-soluble and exchangeable fractions of As were the least abundant of the seven fractions. By comparing the bioavailable fractions of As with those of another enriched heavy metal, cadmium, in karst areas, it was found that the proportion of bioavailable fractions of As was lower than that of cadmium [38]. Furthermore, dendrograms were drawn using a hierarchical cluster analysis to determine the similarities between the different As fractions and rice grains (Figure 4). F1 and F2 were amalgamated as one fraction (F1, F2), owing to their low concentrations. The results indicate a statistical similarity between F1, F2 and the As content in the rice grains. Conversely, no significant similarity was observed between the As content in the rice grains and other fractions, including the total soil As. This implies that the bioavailable fraction (F1, F2) of As in paddy soils is readily absorbed by rice, while massive residual As in paddy soils is hardly absorbed by rice, which causes a low As content in rice grains and a high As content in paddy soils in karst areas.

Table 6. The proportion of As in each fraction by the sequential extraction procedure ($N = 305$).

Fraction	Proportion (%) ^a			
	Min	Max	Median	Mean
Water-soluble (F1)	0.02	7.80	0.38	0.56
Exchangeable (F2)	0.01	3.34	0.37	0.51
Bound to carbonates (F3)	0.03	5.76	0.75	0.97
Weakly bound to organic matter (F4)	0.48	45.03	10.21	11.73
Fe/Mn oxide-bound (F5)	1.11	22.49	7.35	8.07
Strongly bound to organic matter (F6)	0.03	7.10	0.79	1.19
Residual (F7)	37.06	94.56	78.74	76.96

^a Proportion (%): Proportion of each fraction to the sum of the seven fractions.

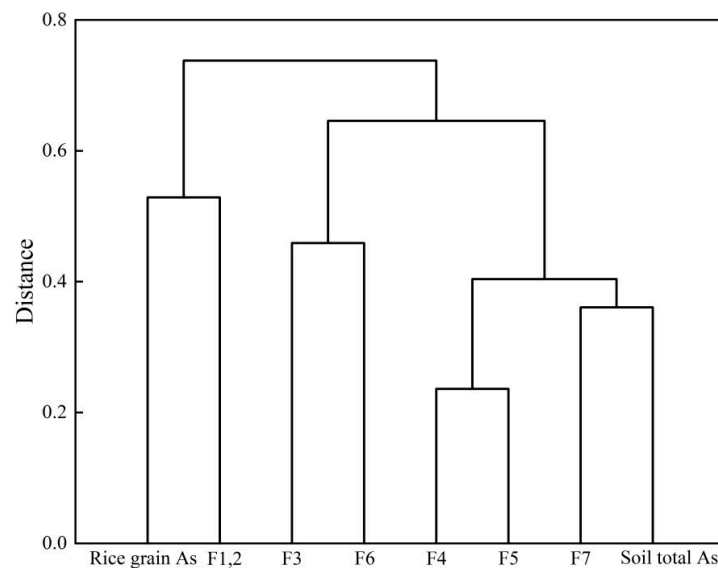


Figure 4. Dendrograms of As in soils and rice grains. F1, F2: water-soluble and exchangeable; F3: bound to carbonates, F4: weakly bound to organic matter, F5: Fe/Mn oxide-bound, F6: strongly bound to organic matter, F7: residual.

3.4. Genesis of Low As Bioavailability in Paddy Soils in Karst Areas

The computed Pearson's correlation values among the soil properties, residual As (F7), and the total soil As are shown in Table 7. Both the total soil As and F7 showed positive correlations with TFe_2O_3 , Mn, and Al_2O_3 , and they showed negative correlations with SiO_2 . Notably, previous research employing field-emission scanning electron microscopy reported that the basic elements in Fe–Mn nodules were Fe, Mn, Al, and Si [28,35].

Table 7. Pearson's correlation coefficients between the soil properties and residual As (F7) ($N = 305$).

	TFe_2O_3	Mn	Al_2O_3	SiO_2	CaO	SOC
Total As	0.664 **	0.579 **	0.449 **	−0.393 **	−0.003	0.051
F7	0.712 **	0.605 **	0.464 **	−0.424 **	0.032	0.067

** at 99% confidence level ($p < 0.01$).

Guangxi encompasses the largest and most distinctive karst landform worldwide [74]. Temperature and rainfall intensify the pedogenesis of carbonate rocks, which includes two stages: leaching accumulation and weathering [27]. The bulk of alkali metals and alkaline earth metals, such as Ca, Mg, and K, leaches from carbonate rocks, whereas Fe, Mn, and Al are retained in and form into (oxyhydr)oxides and minerals, which strongly adsorb As and trace metals, resulting in their comparative enrichment [6,34,71]. These hydrous oxides and some clay minerals gradually dissolve and are repeatedly deposited with

alternating oxidation and reduction, ultimately forming Fe–Mn nodules [75,76]. During later pedogenesis, Fe–Mn nodules are progressively exposed to the ground, along with the strengthening of weathering [38]. The research findings indicate that Fe–Mn nodules accounted for 26.21% of the total amount of soil, and those with diameters lower than 2 mm accounted for 14.18% of the total soil mass in karst areas in Guangxi [28]. As detailed in Table 8, the mean As contents in the Fe–Mn nodules with different diameters were 151.33 mg/kg (0.3–0.5 mm), 188.50 mg/kg (0.5–1 mm), and 201.50 mg/kg (1–2 mm) in the study area, which shows that the As content in Fe–Mn nodules increases rapidly with the particle size. Furthermore, we calculated the contribution of the As, TFe₂O₃, Mn, Al₂O₃, and SiO₂ contents in the Fe–Mn nodules (0.3 mm ≤ diameter ≤ 2 mm) to the host soil, and the results are depicted in Figure 5. The average contribution of As reached 64.45%, with the highest contribution being 82.48%. Additionally, the average contributions of TFe₂O₃, Mn, Al₂O₃, and SiO₂ were 44.38%, 40.17%, 21.57%, and 7.77%, respectively. These results indicate that, as a part of the soil, Fe–Mn nodules play a significant role in the enrichment of As in karst areas.

Table 8. The contents of As, TFe₂O₃, Mn, Al₂O₃, and SiO₂ in the three groups of the Fe–Mn nodules (N = 6).

Groups	Diameter (mm)	Statistics	As (mg/kg)	TFe ₂ O ₃ (%)	Mn (mg/kg)	Al ₂ O ₃ (%)	SiO ₂ (%)
A	0.3–0.5	Min	128.00	25.78	764.00	18.48	14.14
		Max	187.00	30.01	11,640.00	22.04	27.92
		Mid	143.50	26.69	3830.00	20.47	22.00
		Mean	151.33	27.10	5108.00	20.35	21.04
B	0.5–1	Min	158.00	27.67	832.00	18.34	11.55
		Max	253.00	32.55	15,451.00	20.28	20.01
		Mid	175.50	30.03	3296.50	19.23	15.86
		Mean	188.50	30.09	5458.67	19.37	15.81
C	1–2	Min	153.00	27.96	803.00	17.62	10.63
		Max	288.00	32.33	26,331.00	20.51	20.88
		Mid	196.00	31.27	5194.00	19.35	14.77
		Mean	201.50	30.54	9512.00	19.20	15.24

The XRD analysis showed that the Fe–Mn nodules primarily consisted of quartz, goethite, hematite, lithiophorite, birnessite, and phyllosilicates (kaolinite, illite, and clinocllore) (Figure 6). Previous studies have demonstrated that Mn oxide minerals play a primary role in oxidizing As(III) to As(V), which is typically accompanied by the reduction of Mn(IV) to Mn(III) and Mn(II) [77,78]. It was found that the released Mn(II) was easily re-adsorbed at the vacancy sites of Mn oxides until they were completely occupied, which led to the surface passivation of Mn oxides, thereby reducing As adsorption [79]. Iron oxide minerals are recognized as effective adsorbents of As, exhibiting a notably stronger adsorption capacity for As than Mn oxide minerals under isothermal conditions [80]. The X-ray absorption spectroscopy results of the partial environment of As in goethite show that, in addition to the usual bidentate binuclear complex, there is a bidentate mononuclear complex in the absorption, which suggests that As is adsorbed onto the surface of the particles or blocked in the voids and pores [81]. Giménez et al. [82] observed a stronger As(III) adsorption on hematite than on goethite over a broad pH range from 0 to 14. Furthermore, a similar adsorption of As was observed in clay minerals. Lin and Puls [83] investigated six clay minerals, demonstrating that As adsorbed onto clay surfaces can likely infiltrate into the inner pores of clay aggregates, and the dehydration of As residing on clay surfaces could enhance the adherence of As to clays.

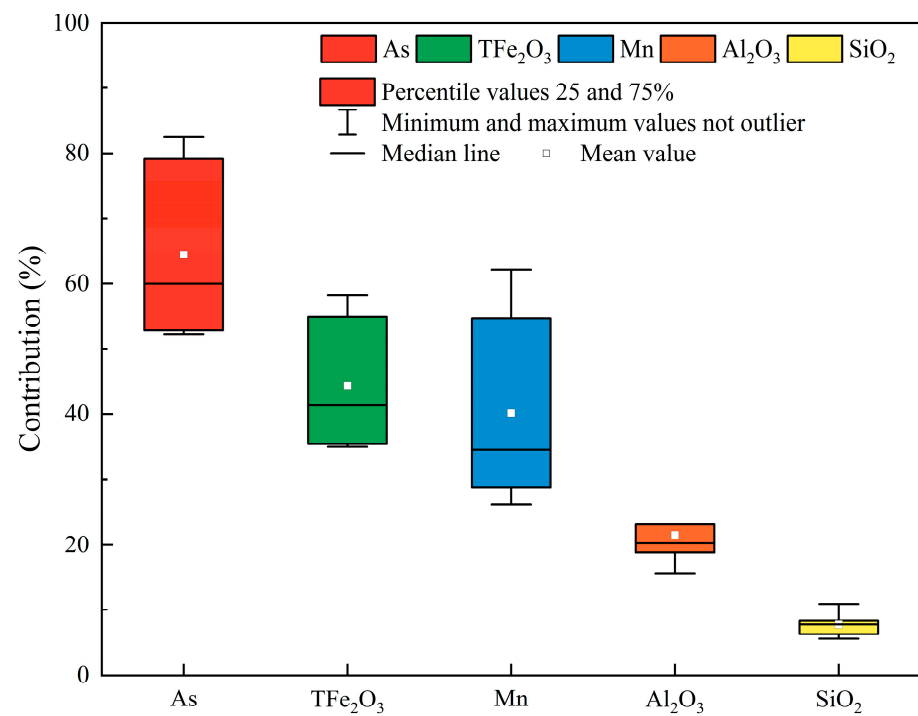


Figure 5. The contributions of As, TFe₂O₃, Mn, Al₂O₃, and SiO₂ in the Fe–Mn nodules (0.3 mm ≤ diameter ≤ 2 mm) to the host soils.

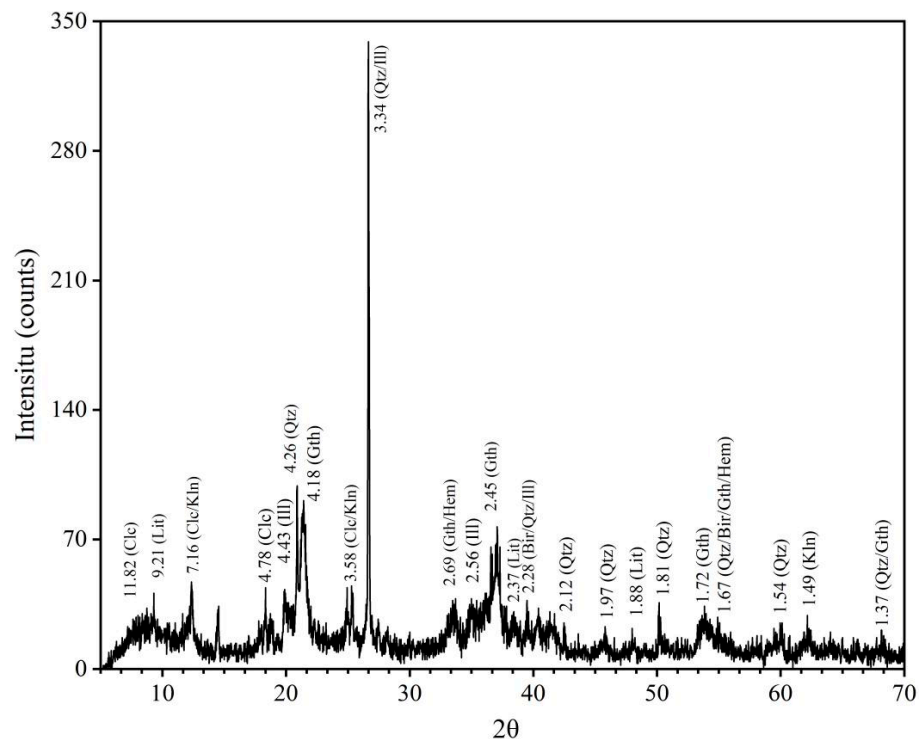


Figure 6. X-ray diffraction patterns of Fe–Mn nodules. Bir, Birnessite; Clc, Clinocllore; Hem, Hematite; Ill, Illite; Gth, Goethite; Kln, Kaolinite; Lit, Lithiophorite; and Qtz, Quartz. Numbers represent the d-values in Å.

To further understand the bioavailability of As in Fe–Mn nodules, the bioavailable As (F1,2) was extracted via the first two steps of SEP. As anticipated, the bioavailable As in the Fe–Mn nodules of three different diameters was negligible, and the extractability was lower

than 0.01%. This suggests that, in karst areas, generous As, tightly adsorbed into Fe–Mn nodules, is barely bioavailable, making it difficult for rice to assimilate it, which may be the ultimate cause of the high content but low bioavailability of As in the paddy soil.

3.5. Stability of Fe–Mn Nodules in the Soil

Selective extraction methods can facilitate the analysis of As distribution within the distinct phases of Fe–Mn nodules. As depicted in Figure 7, HNO₃ dissolved a minor fraction of As (0.78%), Fe (2.35%), Mn (3.63%), and Al (4.16%). NH₂OH-HCl, H₂O₂-HNO₃, and CBD exhibited a strong affinity for Mn, extracting Mn within the range of 64.22–87.01%. However, the extractable As did not show a substantial increase when Mn was significantly dissolved in NH₂OH-HCl. The order of extractability for As and Fe remained consistent: CBD > H₂O₂-HNO₃ > NH₂OH-HCl. Notably, the dissolution of Fe (21.69–67.05%) resulted in a marked increase in As extractability (22.62–51.40%) during CBD extraction. These findings indicate that As within Fe–Mn nodules is predominantly sequestered within Fe-(oxyhydr)oxides, such as goethite and hematite, which exhibit recalcitrance and remain undissolved. Arsenic associated with amorphous iron oxides can undergo dissolution through acid-enhanced, reductive, and chelant-enhanced mechanisms [43,44], while As bound to crystalline iron oxides can only be dissolved via reductive processes [84]. CBD, functioning as a potent reducing agent, triggers the reductive dissolution of crystalline iron oxides [44]. In essence, under strongly reducing conditions in the soil (i.e., hypoxia), the reductive dissolution of Fe-(oxyhydr)oxides within Fe–Mn nodules can release As into the soil solution, potentially enhancing the uptake of As by rice [85,86].

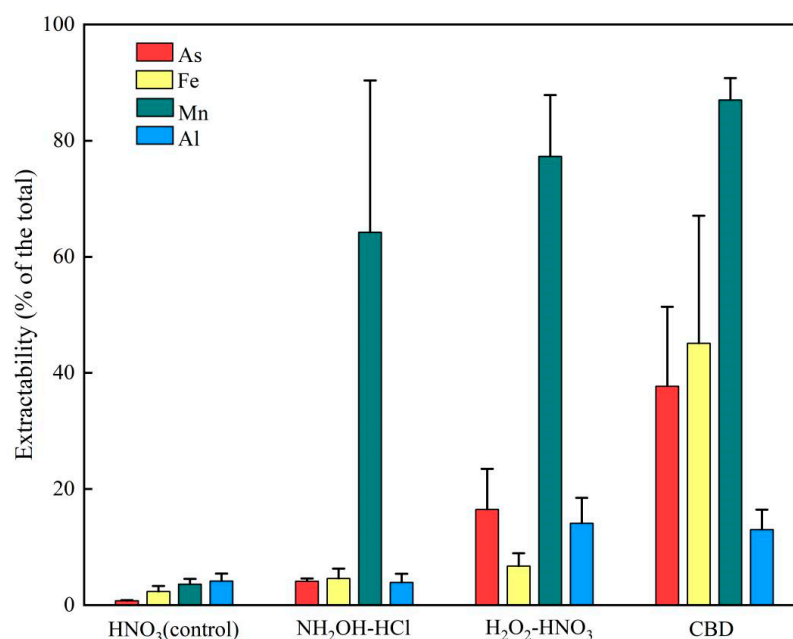


Figure 7. Dissolution of As, Fe, Mn, and Al from Fe–Mn nodules using different selective extractions.

The findings of the pH-dependent leaching assessments are depicted in Figure 8. Across a pH range from 2 to 11, the overall leaching of As remained notably low. At pH 2, the leached concentration of As was 0.05 mg/kg, constituting a mere 0.02% of the total concentrations within the Fe–Mn nodules. Similarly, at pH 11, the leached As concentration was 0.03 mg/kg, accounting for 0.01%. The dissolved As concentrations at other pH levels (3–10) were all less than 0.01% of the total concentrations in the Fe–Mn nodules, rendering them nearly negligible. Moreover, the trend of As variation mirrored that of Fe, underscoring the close association between As and Fe within the Fe–Mn nodules. In essence, the results suggest that Fe–Mn nodules exhibit a robust stability in storing As, with extremely acidic or alkaline conditions promoting the potential release of As from the

nodules due to the desorption or dissolution of the Fe-(oxyhydr)oxides. The pH range of the karstic paddy soil (4.97–8.38) provides favorable conditions for the preservation of As within the Fe–Mn nodules.

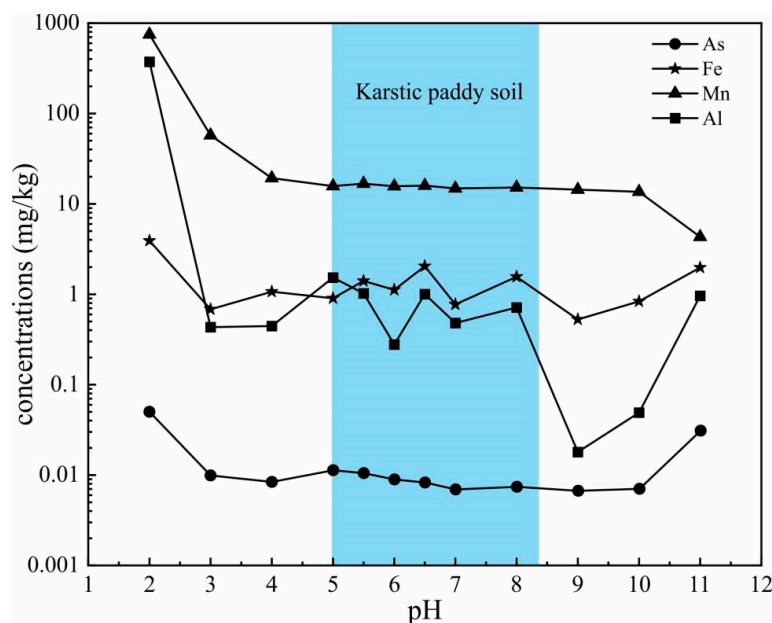


Figure 8. The pH-dependent leaching of As, Fe, Mn, and Al from Fe–Mn nodules. The blue area is the portion with a pH of 4.97–8.38.

4. Conclusions

The paddy soil in karst areas exhibited a higher geochemical background of As, with the concentration significantly surpassing that found in non-karst regions. However, the As concentration in the rice grains within the karst area remained low, with only 0.62% of the rice samples exceeding the permissible value for inorganic As (0.2 mg/kg). The SEP results show that As in the karstic paddy soil is present mostly in the residual fraction, and the water-soluble and exchangeable fractions of As, readily absorbed by rice, are extremely rare. The high As content but low bioavailability of As in the karstic paddy soil can be primarily attributed to the abundant Fe–Mn nodules, which adsorbed and immobilized a significant portion of As, contributing to 64.45% of the As content in the host soil. The bioavailable fraction of As was found to be less than 0.01% of the total As in the Fe–Mn nodules. Selective extractions revealed that As was primarily sequestered within Fe-(oxyhydr)oxides, which could release As into the soil under certain reduction conditions through the reductive dissolution of Fe-(oxyhydr)oxides. pH-dependent leaching tests showed that only under extremely acidic (pH = 2) and alkaline (pH = 11) conditions was there a trend of As leaching from the Fe–Mn nodules. In the natural pH range of the karstic paddy soil (pH 4.97–8.38), As remained steadily adhered to the Fe–Mn nodules. Therefore, agricultural soil quality management in karst areas should not only be based on the total As content in the soil but should also consider the bioavailability of As, thereby tailoring adaptations to fully utilize arable land.

Author Contributions: X.L. (Xuezhen Li): Conceptualization, Methodology, Formal analysis, Writing original—draft, Writing—review and editing, and Visualization. X.M.: Methodology, Formal analysis, and Visualization. Q.H.: Writing—review and editing, and Supervision. X.X.: Supervision. B.L.: Investigation and Resources. K.L.: Investigation and Resources. X.L. (Xu Liu): Investigation and Resources. Z.W.: Investigation and Resources. W.J.: Data curation. L.W.: Resources. T.Y.: Conceptualization, Writing—review and editing, Supervision, Project administration, and Funding acquisition. Z.Y.: Conceptualization, Writing—review and editing, Supervision, and Funding acquisition. All authors have read and agreed to the published version of the manuscript.

Funding: This work was financially supported by the Geological Survey Project of China (Grant No. DD20211414) and the National Natural Science Foundation of China (42330703).

Data Availability Statement: The data presented in this study are available upon request from the corresponding author. The data are not publicly available due to the confidentiality of the project.

Acknowledgments: The authors appreciate the helpful and useful suggestions of the editors and reviewers.

Conflicts of Interest: The authors declare no conflicts of interest.

References

1. Wei, B.G.; Yang, L.S. A review of heavy metal contaminations in urban soils, urban road dusts and agricultural soils from China. *Microchem. J.* **2010**, *94*, 99–107. [[CrossRef](#)]
2. Li, C.J.; Wang, J.H.; Yan, B.; Miao, A.J.; Zhong, H.; Zhang, W.; Ma, L.Q. Progresses and emerging trends of arsenic research in the past 120 years. *Crit. Rev. Environ. Sci. Technol.* **2021**, *51*, 1306–1353. [[CrossRef](#)]
3. Bundschuh, J.; Armienta, M.A.; Morales-Simfors, N.; Alam, M.A.; López, D.L.; Quezada, V.D.; Dietrich, S.; Schneider, J.; Tapia, J.; Sracek, O.; et al. Arsenic in Latin America: New findings on source, mobilization and mobility in human environments in 20 countries based on decadal research 2010–2020. *Crit. Rev. Environ. Sci. Technol.* **2021**, *51*, 1727–1865. [[CrossRef](#)]
4. Alexakis, D.E.; Bathrellos, G.D.; Skilodimou, H.D.; Gamvroula, D.E. Spatial Distribution and Evaluation of Arsenic and Zinc Content in the Soil of a Karst Landscape. *Sustainability* **2021**, *13*, 6976. [[CrossRef](#)]
5. Zhao, F.J.; Ma, Y.B.; Zhu, Y.G.; Tang, Z.; McGrath, S.P. Soil Contamination in China: Current Status and Mitigation Strategies. *Environ. Sci. Technol.* **2015**, *49*, 750–759. [[CrossRef](#)]
6. Yang, Q.; Yang, Z.F.; Filippelli, G.M.; Ji, J.F.; Ji, W.B.; Liu, X.; Wang, L.; Yu, T.; Wu, T.S.; Zhuo, X.X.; et al. Distribution and secondary enrichment of heavy metal elements in karstic soils with high geochemical background in Guangxi, China. *Chem. Geol.* **2021**, *567*, 120081. [[CrossRef](#)]
7. Mombo, S.; Foucault, Y.; Deola, F.; Gaillard, I.; Goix, S.; Shahid, M.; Schreck, E.; Pierart, A.; Dumat, C. Management of human health risk in the context of kitchen gardens polluted by lead and cadmium near a lead recycling company. *J. Soil Sediment* **2016**, *16*, 1214–1224. [[CrossRef](#)]
8. Chen, J.; Garbinski, L.D.; Rosen, B.; Zhang, J.; Xiang, P.; Ma, L.Q. Organoarsenical compounds: Occurrence, toxicology and biotransformation. *Crit. Rev. Environ. Sci. Technol.* **2020**, *50*, 217–243. [[CrossRef](#)]
9. Li, H.B.; Li, M.Y.; Zhao, D.; Li, J.; Li, S.W.; Xiang, P.; Juhsaz, A.L.; Ma, L.N.Q. Arsenic, lead, and cadmium bioaccessibility in contaminated soils: Measurements and validations. *Crit. Rev. Environ. Sci. Technol.* **2020**, *50*, 1303–1338. [[CrossRef](#)]
10. Chen, H.Y.; Teng, Y.G.; Lu, S.J.; Wang, Y.Y.; Wang, J.S. Contamination features and health risk of soil heavy metals in China. *Sci. Total Environ.* **2015**, *512*, 143–153. [[CrossRef](#)]
11. Gu, Q.B.; Yang, Z.F.; Yu, T.; Ji, J.F.; Hou, Q.Y.; Zhang, Q.Z. Application of ecogeochemical prediction model to safely exploit seleniferous soil. *Ecotoxicol. Environ. Safe* **2019**, *177*, 133–139. [[CrossRef](#)]
12. Xiao, J.; Chen, W.; Wang, L.; Zhang, X.K.; Wen, Y.B.; Bostick, B.C.; Wen, Y.L.; He, X.H.; Zhang, L.Y.; Zhuo, X.X.; et al. New strategy for exploring the accumulation of heavy metals in soils derived from different parent materials in the karst region of southwestern China. *Geoderma* **2022**, *417*, 115806. [[CrossRef](#)]
13. Lu, A.X.; Wang, J.H.; Qin, X.Y.; Wang, K.Y.; Han, P.; Zhang, S.Z. Multivariate and geostatistical analyses of the spatial distribution and origin of heavy metals in the agricultural soils in Shunyi, Beijing, China. *Sci. Total Environ.* **2012**, *425*, 66–74. [[CrossRef](#)]
14. Yamasaki, S.; Takeda, A.; Nunohara, K.; Tsuchiya, N. Red soils derived from limestone contain higher amounts of trace elements than those derived from various other parent materials. *Soil Sci. Plant Nutr.* **2013**, *59*, 692–699. [[CrossRef](#)]
15. Yang, Q.; Yang, Z.F.; Zhang, Q.Z.; Ji, W.B.; Guan, D.X.; Liu, X.; Yu, T.; Wang, L.; Zhuo, X.X.; Ji, J.F. Transferability of heavy metal(loid)s from karstic soils with high geochemical background to peanut seeds. *Environ. Pollut.* **2022**, *299*, 118819. [[CrossRef](#)] [[PubMed](#)]
16. *GB 15618-2018*; Soil Environmental Quality—Risk Control Standards for Soil Contamination of Agricultural Land. MEEC (Ministry of Ecology and Environment of the People’s Republic of China): Beijing, China, 2018.
17. Xia, X.Q.; Ji, J.F.; Zhang, C.S.; Yang, Z.F.; Shi, H.D. Carbonate bedrock control of soil Cd background in Southwestern China: Its extent and influencing factors based on spatial analysis. *Chemosphere* **2022**, *290*, 133390. [[CrossRef](#)] [[PubMed](#)]
18. Peijnenburg, W.; Baerselman, R.; de Groot, A.; Jager, T.; Leenders, D.; Posthuma, L.; Van Veen, R. Quantification of metal bioavailability for lettuce (*Lactuca sativa* L.) in field soils. *Arch. Environ. Contam. Toxicol.* **2000**, *39*, 420–430. [[CrossRef](#)] [[PubMed](#)]
19. Wenzel, W.W.; Kirchbaumer, N.; Prohaska, T.; Stingeder, G.; Lombi, E.; Adriano, D.C. Arsenic fractionation in soils using an improved sequential extraction procedure. *Anal. Chim. Acta.* **2001**, *436*, 309–323. [[CrossRef](#)]
20. Adamo, P.; Iavazzo, P.; Albanese, S.; Agrelli, D.; De Vivo, B.; Lima, A. Bioavailability and soil-to-plant transfer factors as indicators of potentially toxic element contamination in agricultural soils. *Sci. Total Environ.* **2014**, *500*, 11–22. [[CrossRef](#)] [[PubMed](#)]
21. Zhang, J.R.; Li, H.Z.; Zhou, Y.Z.; Dou, L.; Cai, L.M.; Mo, L.P.; You, J. Bioavailability and soil-to-crop transfer of heavy metals in farmland soils: A case study in the Pearl River Delta, South China. *Environ. Pollut.* **2018**, *235*, 710–719. [[CrossRef](#)] [[PubMed](#)]

22. Luo, H.; Liu, X.M.; Wang, S.J.; Liu, F.; Li, Y. Pollution characteristics and sources of cadmium in soils of the karst area in South China. *Chin. J. Ecol.* **2018**, *37*, 1538–1544. [[CrossRef](#)]
23. Zhang, F.G.; Peng, M.; Wan, H.Y.; Ma, H.H.; Xu, R.T.; Cheng, X.M.; Hou, Z.L.; Chen, Z.F.; Li, K.; Cheng, H.X. Ecological risk assessment of heavy metals at township scale in the high background of heavy metals, southwestern China. *Environ. Sci.* **2020**, *41*, 4197–4209. [[CrossRef](#)]
24. Tu, C.L.; He, T.B.; Liu, C.Q.; Lu, X.H. Effects of Land Use and Parent Materials on Trace Elements Accumulation in Topsoil. *J. Environ. Qual.* **2013**, *42*, 103–110. [[CrossRef](#)] [[PubMed](#)]
25. Chang, C.; Li, F.; Wang, Q.; Hu, M.; Du, Y.; Zhang, X.; Zhang, X.; Chen, C.; Yu, H.-Y. Bioavailability of antimony and arsenic in a flowering cabbage–soil system: Controlling factors and interactive effect. *Sci. Total Environ.* **2022**, *815*, 152920. [[CrossRef](#)]
26. Kwon, J.C.; Nejad, Z.D.; Jung, M.C. Arsenic and heavy metals in paddy soil and polished rice contaminated by mining activities in Korea. *Catena* **2017**, *148*, 92–100. [[CrossRef](#)]
27. Wang, Y.Z.; Yu, T.; Yang, Z.F.; Bo, H.Z.; Lin, Y.; Yang, Q.; Liu, X.; Zhang, Q.Z.; Zhuo, X.X.; Wu, T.S. Zinc concentration prediction in rice grain using back-propagation neural network based on soil properties and safe utilization of paddy soil: A large-scale field study in Guangxi, China. *Sci. Total Environ.* **2021**, *798*, 149270. [[CrossRef](#)] [[PubMed](#)]
28. Ji, W.B.; Yang, Z.F.; Yu, T.; Yang, Q.; Wen, Y.B.; Wu, T.S. Potential Ecological Risk Assessment of Heavy Metals in the Fe-Mn Nodules in the Karst Area of Guangxi, Southwest China. *Bull. Environ. Contam. Toxicol.* **2021**, *106*, 51–56. [[CrossRef](#)]
29. Feng, Y.F.; Liao, Q.L.; Ji, W.B.; Ren, J.L.; Ji, J.F.; Yang, Z.F. Geochemical Characteristics of Heavy Metal Enrichment in Soil Fe-Mn Nodules in the Karst Area of Guangxi. *Geol. J. China Univ.* **2022**, *28*, 787–798. [[CrossRef](#)]
30. Gasparatos, D. *Fe–Mn Concretions and Nodules to Sequester Heavy Metals in Soils*; Springer: Houten, The Netherlands, 2012. [[CrossRef](#)]
31. Li, Y.L.; Li, P.Y.; Liu, L.N. Source Identification and Potential Ecological Risk Assessment of Heavy Metals in the Topsoil of the Weining Plain (Northwest China). *Expos. Health* **2022**, *14*, 281–294. [[CrossRef](#)]
32. MNR (Ministry of Land and Resources of the People’s Republic of China). *Regional Geochemical Sample Analysis Method—Part 27: Potassium Dichromate Capacity Method. DZ/T 0279.27-2016.0. and Part 34: Determination of pH Values Ion Selection Electrode Method DZ/T 0279.34-2016.0*; China University of Geosciences Press: Beijing, China, 2016.
33. Ji, W.; Ying, R.; Yang, Z.; Hu, Z.; Yang, Q.; Liu, X.; Yu, T.; Wang, L.; Qin, J.; Wu, T. Arsenic Concentration, Fraction, and Environmental Implication in Fe–Mn Nodules in the Karst Area of Guangxi. *Water* **2022**, *14*, 3021. [[CrossRef](#)]
34. Yu, X.L.; Fu, Y.N.; Brookes, P.C.; Lu, S.G. Insights into the Formation Process and Environmental Fingerprints of Iron-Manganese Nodules in Subtropical Soils of China. *Soil Sci. Soc. Am. J.* **2015**, *79*, 1101–1114. [[CrossRef](#)]
35. Ettler, V.; Chren, M.; Mihaljevič, M.; Drahotka, P.; Kříbek, B.; Veselovský, F.; Sracek, O.; Vaněk, A.; Penížek, V.; Komárek, M.; et al. Characterization of Fe-Mn concentric nodules from Luvisol irrigated by mine water in a semi-arid agricultural area. *Geoderma* **2017**, *299*, 32–42. [[CrossRef](#)]
36. Li, X.Z.; Hou, Q.Y.; Duan, Y.R.; Li, Y.C.; Lin, K.; Li, B.; Sheng, W.K.; Wang, Y.L.; Su, R.; Gu, Z.L.; et al. Soil selenium enrichment in the Loess Plateau of China: Geogenic evidence, spatial distribution, and its influence factors. *Chemosphere* **2023**, *340*, 139746. [[CrossRef](#)]
37. CGS (China Geological Survey). *China Geological Survey Bureau Geological Survey Technical Standard—The Technical Requirements for Eco-Geochemical Analysis of Sample (DD2005-03)*; CGS (China Geological Survey): Beijing, China, 2005.
38. Li, C.; Yang, Z.F.; Yu, T.; Hou, Q.Y.; Liu, X.; Wang, J.; Zhang, Q.Z.; Wu, T.S. Study on safe usage of agricultural land in karst and non-karst areas based on soil Cd and prediction of Cd in rice: A case study of Heng County, Guangxi. *Ecotoxicol. Environ. Saf.* **2021**, *208*, 111505. [[CrossRef](#)]
39. Houben, D.; Evrard, L.; Sonnet, P. Mobility, bioavailability and pH-dependent leaching of cadmium, zinc and lead in a contaminated soil amended with biochar. *Chemosphere* **2013**, *92*, 1450–1457. [[CrossRef](#)]
40. Stigliani, W.M.; Doelman, P.; Salomons, W.; Schulin, R.; Smidt, G.R.B.; Vanderzee, S.E.A.T.M. Chemical Time Bombs—Predicting the Unpredictable. *Environment* **1991**, *33*, 4. [[CrossRef](#)]
41. Neaman, A.; Mouélé, F.; Trolard, F.; Bourrié, G. Improved methods for selective dissolution of Mn oxides: Applications for studying trace element associations. *Appl. Geochem.* **2004**, *19*, 973–979. [[CrossRef](#)]
42. Neaman, A.; Waller, B.; Mouélé, F.; Trolard, F.; Bourrié, G. Improved methods for selective dissolution of manganese oxides from soils and rocks. *Eur. J. Soil Sci.* **2004**, *55*, 47–54. [[CrossRef](#)]
43. Zhang, X.; Dayton, E.A.; Basta, N.T. Predicting the modifying effect of soils on arsenic phytotoxicity and phytoaccumulation using soil properties or soil extraction methods. *Environ. Pollut.* **2020**, *263*, 114501. [[CrossRef](#)] [[PubMed](#)]
44. Lee, M.E.; Jeon, E.K.; Tsang, D.C.W.; Baek, K. Simultaneous application of oxalic acid and dithionite for enhanced extraction of arsenic bound to amorphous and crystalline iron oxides. *J. Hazard. Mater.* **2018**, *354*, 91–98. [[CrossRef](#)] [[PubMed](#)]
45. CEN/TS 14997; Characterization of Waste-Leaching Behaviour Tests—Influence of pH on Leaching with Continuous pH-Control. CEN: Brussels, Belgium, 2006.
46. Chopra, A.K.; Pathak, C. *Accumulation of Heavy Metals in the Vegetables Grown in Wastewater Irrigated Areas of Dehradun, India with Reference to Human Health Risk*; Department of Zoology and Environmental Science, Gurukula Kangri University: Haridwar, India, 2015; Volume 187, pp. 1–16. [[CrossRef](#)]
47. Torralba-Sanchez, T.; Kuo, D.; Allen, H.; Di Toro, D. Bioconcentration factors and plant–water partition coefficients of munitions compounds in barley. *Chemosphere* **2017**, *189*, 538–546. [[CrossRef](#)]

48. Yang, Q.; Yang, Z.F.; Ji, J.F.; Liu, X.; Ji, W.B.; Wang, J.; Wu, T.S.; Wang, L. Characteristics of Mineralogy and Heavy Metal Geochemistry in Ferromanganese Nodule Rich Soils with High Geochemical Background from Guigang, Guangxi. *Geoscience* **2021**, *35*, 1450–1458. [[CrossRef](#)]
49. Yang, Q.; Yang, Z.F.; Zhang, Q.Z.; Liu, X.; Zhuo, X.X.; Wu, T.S.; Wang, L.; Wei, X.J.; Ji, J.F. Ecological risk assessment of Cd and other heavy metals in soil-rice system in the karst areas with high geochemical background of Guangxi, China. *Sci. China Earth Sci.* **2021**, *64*, 1126–1139. [[CrossRef](#)]
50. Hou, Q.Y.; Yang, Z.F.; Yu, T.; Xia, X.Q.; Cheng, H.X.; Zhou, G.H. *Soil Geochemical Dataset of China*; Geological Publishing House: Beijing, China, 2020; pp. 2656–2668.
51. Akun, M.E.; Yamaci, R.F.; Charalambous, C.; Lechtvich, S.; Djamgoz, M. The distribution of carcinogenic heavy metals in cyprus soil. In *Environmental Earth Sciences-Series*; Springer: Berlin/Heidelberg, Germany, 2010; pp. 353–359. [[CrossRef](#)]
52. Marchant, B.P.; Saby, N.P.A.; Arrouays, D. A survey of topsoil arsenic and mercury concentrations across France. *Chemosphere* **2017**, *181*, 635–644. [[CrossRef](#)]
53. Ungaro, F.; Ragazzi, F.; Cappellin, R.; Giandon, P. Arsenic concentration in the soils of the Brenta Plain (Northern Italy): Mapping the probability of exceeding contamination thresholds. *J. Geochem. Explor.* **2008**, *96*, 117–131. [[CrossRef](#)]
54. Golfopoulos, S.K.; Varnavas, S.P.; Alexakis, D.E. The Status of Arsenic Pollution in the Greek and Cyprus Environment: An Overview. *Water* **2021**, *13*, 224. [[CrossRef](#)]
55. Ma, L.; Wang, L.; Jia, Y.; Yang, Z. Arsenic speciation in locally grown rice grains from Hunan Province, China: Spatial distribution and potential health risk. *Sci. Total Environ.* **2016**, *557–558*, 438–444. [[CrossRef](#)] [[PubMed](#)]
56. Fu, Y.; Chen, M.; Bi, X.; He, Y.; Ren, L.; Xiang, W.; Qiao, S.; Yan, S.; Li, Z.; Ma, Z. Occurrence of arsenic in brown rice and its relationship to soil properties from Hainan Island, China. *Environ. Pollut.* **2011**, *159*, 1757–1762. [[CrossRef](#)] [[PubMed](#)]
57. Huang, R.; Gao, S.; Wang, W.; Staunton, S.; Wang, G. Soil arsenic availability and the transfer of soil arsenic to crops in suburban areas in Fujian Province, southeast China. *Sci. Total Environ.* **2006**, *368*, 531–541. [[CrossRef](#)] [[PubMed](#)]
58. Meharg, A.A.; Williams, P.N.; Adomako, E.; Lawgali, Y.Y.; Deacon, C.; Villada, A.; Cambell, R.C.J.; Sun, G.; Zhu, Y.G.; Feldmann, J.; et al. Geographical Variation in Total and Inorganic Arsenic Content of Polished (White) Rice. *Environ. Sci. Technol.* **2009**, *43*, 1612–1617. [[CrossRef](#)]
59. Mahar, A.; Wang, P.; Ali, A.; Guo, Z.Y.; Awasthi, M.K.; Lahori, A.H.; Wang, Q.; Shen, F.; Zhang, Z.Q. Impact of CaO, fly ash, sulfur and Na₂S on the (im)mobilization and phytoavailability of Cd, Cu and Pb in contaminated soil. *Ecotoxicol. Environ. Saf.* **2016**, *134*, 116–123. [[CrossRef](#)] [[PubMed](#)]
60. Khan, I.; Awan, S.A.; Rizwan, M.; Ali, S.; Zhang, X.Q.; Huang, L.K. Arsenic behavior in soil-plant system and its detoxification mechanisms in plants: A review. *Environ. Pollut.* **2021**, *286*, 117389. [[CrossRef](#)] [[PubMed](#)]
61. Williams, P.N.; Zhang, H.; Davison, W.; Meharg, A.A.; Hossain, M.; Norton, G.J.; Brammer, H.; Islam, M.R. Organic Matter-Solid Phase Interactions Are Critical for Predicting Arsenic Release and Plant Uptake in Bangladesh Paddy Soils. *Environ. Sci. Technol.* **2011**, *45*, 6080–6087. [[CrossRef](#)] [[PubMed](#)]
62. Yan, M.M.; Zeng, X.B.; Wang, J.; Meharg, A.A.; Meharg, C.; Tang, X.J.; Zhang, L.L.; Bai, L.Y.; Zhang, J.Z.; Su, S.M. Dissolved organic matter differentially influences arsenic methylation and volatilization in paddy soils. *J. Hazard. Mater.* **2020**, *388*, 121795. [[CrossRef](#)] [[PubMed](#)]
63. Meharg, A.A.; Meharg, C.; Carey, M.; Williams, P.; Shi, Z.Y.; Campbell, K.; Elliott, C.; Marwa, E.; Xiao, J.J.; Farias, J.G.; et al. Global Geographical Variation in Elemental and Arsenic Species Concentration in Paddy Rice Grain Identifies a Close Association of Essential Elements Copper, Selenium and Molybdenum with Cadmium. *Expos. Health* **2022**, *15*, 505–518. [[CrossRef](#)]
64. GB2762-2017; Maximum Level of Contaminants in Food. MHC (Ministry of Health of the People's Republic of China) Chinese National Standard Agency: Beijing, China, 2017.
65. Williams, P.N.; Price, A.H.; Raab, A.; Hossain, S.A.; Feldmann, J.; Meharg, A.A. Variation in arsenic speciation and concentration in paddy rice related to dietary exposure. *Environ. Sci. Technol.* **2005**, *39*, 5531–5540. [[CrossRef](#)]
66. Zhao, F.; Zhu, Y.; Meharg, A. Methylated Arsenic Species in Rice: Geographical Variation, Origin, and Uptake Mechanisms. *Environ. Sci. Technol.* **2013**, *47*, 3957–3966. [[CrossRef](#)]
67. Armendariz, A.L.; Talano, M.A.; Travaglia, C. Arsenic toxicity in soybean seedlings and their attenuation mechanisms. *Plant Physiol. Biochem.* **2016**, *98*, 119–127. [[CrossRef](#)]
68. Siddiqui, M.H.; Alamri, S.; Khan, M.N.; Corpas, F.J.; Al-Amri, A.A.; Alsubaie, Q.D.; Ali, H.M.; Kalaji, H.M.; Ahmad, P. Melatonin and calcium function synergistically to promote the resilience through ROS metabolism under arsenic-induced stress. *J. Hazard. Mater.* **2020**, *398*, 122882. [[CrossRef](#)]
69. Xue, X.M.; Xiong, C.; Yoshinaga, M.; Rosen, B.; Zhu, Y.G. The enigma of environmental organoarsenicals. *Crit. Rev. Environ. Sci. Technol.* **2021**, *1–28*.
70. Du, X.; Gao, L.; Xun, Y.; Feng, L. Comparison of different sequential extraction procedures to identify and estimate bioavailability of arsenic fractions in soil. *J. Soil Sediments* **2020**, *20*, 3656–3668. [[CrossRef](#)]
71. Yamaguchi, N.; Nakamura, T.; Dong, D.; Takahashi, Y.; Amachi, S.; Makino, T. Arsenic release from flooded paddy soils is influenced by speciation, Eh, pH, and iron dissolution. *Chemosphere* **2011**, *83*, 925–932. [[CrossRef](#)]
72. Srithongkul, C.; Wongsaiapun, S.; Krongchai, C.; Santasup, C.; Kittiwachana, S. Investigation of mobility and bioavailability of arsenic in agricultural soil after treatment by various soil amendments using sequential extraction procedure and multivariate analysis. *Catena* **2019**, *181*, 104084. [[CrossRef](#)]

73. Malandrino, M.; Abollino, O.; Buoso, S.; Giacomino, A.; La Gioia, C.; Mentasti, E. Accumulation of heavy metals from contaminated soil to plants and evaluation of soil remediation by vermiculite. *Chemosphere* **2011**, *82*, 169–178. [[CrossRef](#)]
74. Jia, Z.Y.; Wang, J.X.; Zhou, X.D.; Zhou, Y.J.; Li, Y.; Li, B.J.; Zhou, S.L. Identification of the sources and influencing factors of potentially toxic elements accumulation in the soil from a typical karst region in Guangxi, Southwest China. *Environ. Pollut.* **2020**, *256*, 113505. [[CrossRef](#)]
75. Gao, T.; Ke, S.; Wang, S.; Li, F.; Liu, C.; Lei, J.; Liao, C.; Wu, F. Contrasting Mg isotopic compositions between Fe-Mn nodules and surrounding soils: Accumulation of light Mg isotopes by Mg-depleted clay minerals and Fe oxides. *Geochim. Cosmochim. Acta* **2018**, *237*, 205–222. [[CrossRef](#)]
76. Wei, X.; Ji, H.B.; Wang, S.J.; Chu, H.S.; Song, C.S. The formation of representative lateritic weathering covers in south-central Guangxi (southern China). *Catena* **2014**, *118*, 55–72. [[CrossRef](#)]
77. Suda, A.; Makino, T. Functional effects of manganese and iron oxides on the dynamics of trace elements in soils with a special focus on arsenic and cadmium: A review. *Geoderma* **2016**, *270*, 68–75. [[CrossRef](#)]
78. Zhang, G.S.; Qu, J.H.; Liu, H.J.; Liu, R.P.; Li, G.T. Removal mechanism of As(III) by a novel Fe-Mn binary oxide adsorbent: Oxidation and sorption. *Environ. Sci. Technol.* **2007**, *41*, 4613–4619. [[CrossRef](#)]
79. Rady, O.; Liu, L.H.; Yang, X.; Tang, X.J.; Tan, W.F.; Qiu, G.H. Adsorption and catalytic oxidation of arsenite on Fe-Mn nodules in the presence of oxygen. *Chemosphere* **2020**, *259*, 127503. [[CrossRef](#)] [[PubMed](#)]
80. Violante, A.; Pigna, M. Competitive sorption of arsenate and phosphate on different clay minerals and soils. *Soil Sci. Soc. Am. J.* **2002**, *66*, 1788–1796. [[CrossRef](#)]
81. Jerzykowska, I.; Majzlan, J.; Michalik, M.; Göttlicher, J.; Steininger, R.; Błachowski, A.; Ruebenbauer, K. Mineralogy and speciation of Zn and As in Fe-oxide-clay aggregates in the mining waste at the MVT Zn–Pb deposits near Olkusz, Poland. *Geochemistry* **2014**, *74*, 393–406. [[CrossRef](#)]
82. Giménez, J.; Martínez, M.; Depablo, J.; Rovira, M.; Duro, L. Arsenic sorption onto natural hematite, magnetite, and goethite. *J. Hazard. Mater.* **2007**, *141*, 575–580. [[CrossRef](#)] [[PubMed](#)]
83. Lin, Z.; Puls, R.W. Adsorption, desorption and oxidation of arsenic affected by clay minerals and aging process. *Environ. Geol.* **2000**, *39*, 753–759. [[CrossRef](#)]
84. Anschutz, A.J.; Penn, R.L. Reduction of crystalline iron(III) oxyhydroxides using hydroquinone: Influence of phase and particle size. *Geochem. Trans.* **2005**, *6*, 60–66. [[CrossRef](#)]
85. Kocar, B.D.; Borch, T.; Fendorf, S. Arsenic repartitioning during biogenic sulfidization and transformation of ferrihydrite. *Geochim. Cosmochim. Acta* **2010**, *74*, 980–994. [[CrossRef](#)]
86. Smedley, P.L.; Kinniburgh, D.G. A review of the source, behaviour and distribution of arsenic in natural waters. *Appl. Geochem.* **2002**, *17*, 517–568. [[CrossRef](#)]

Disclaimer/Publisher’s Note: The statements, opinions and data contained in all publications are solely those of the individual author(s) and contributor(s) and not of MDPI and/or the editor(s). MDPI and/or the editor(s) disclaim responsibility for any injury to people or property resulting from any ideas, methods, instructions or products referred to in the content.